INTERFACE SCIENCE 11, 319–327, 2003

Interfacial Debonding Around Rectangular Features in Multilayer Structures

MATTHEW R. BEGLEY*
Structural and Solid Mechanics, Department of Civil Engineering, University of Virginia, Charlottesville, VA 22904, USA
begley@virginia.edu

CHRISTOPHER J. BEGLEY
TCA Solutions, LLC, Charlottesville, VA 22947, USA

Abstract. This article describes a numerical approach for predicting debonding in multi-layers comprised of rectangular features of different sizes. A single global meshing strategy for finite element analysis is described that includes focused radial meshes at every material junction to accurately capture crack tip and material junction singularities. The strategy is designed to allow straightforward yet accurate calculations of energy release rates for steady-state interfacial debonding in complex architectures. Guidelines for meshing parameters (such as element density and distribution) are discussed on the basis of convergence studies of stress distributions along interface junctions, crack opening displacements and crack driving forces along interfaces. The utility of the approach is demonstrated via a study of debonding around rectangular inclusions, which illustrates relationships between energy release rates, inclusion aspect ratio and elastic mismatch. The paper concludes with an illustration of how interfacial debonding along finite-sized features can promote cracking in adjacent layers.

Keywords: debonding, multilayers, junction singularities, finite element modeling

1. Introduction

Most analyses of interface debonding in multi-layered systems have been limited to blanket films or laminates, wherein each disparate material section consists of a semi-infinite sheet whose only finite dimension is thickness (e.g. [1, 2]). Such film/laminate analyses are effective in identifying the fundamental mechanics underlying reliability; however, they often miss important interactions between disparate material sections that have a large impact on interface failures in real systems (e.g. [3]). Many applications have finite-sized features that are not accurately idealized as blanket films—i.e. features whose in-plane dimensions are comparable to thickness (e.g. [4]). This is particularly true for microelectronics, both at the scale of individual features on a chip and on the scale of encapsulated packages comprised of many microchips. Typical cross-sections of these systems involve rectangular sections, as shown schematically in Fig. 1.

The growing complexity of such composite structures and the implementation of new materials with reduced mechanical properties (such as polymers and porous glass) has created a critical need for a general analysis approach capable of considering a wide range of feature characteristics and material behavior [4]. Approaches that incorporate finite feature sizes allow for rapid evaluation of new materials and architectures *a priori*, in contrast to "fabricate-and-function" empirical approaches to determining mechanical stability.

*To whom all correspondence should be addressed.

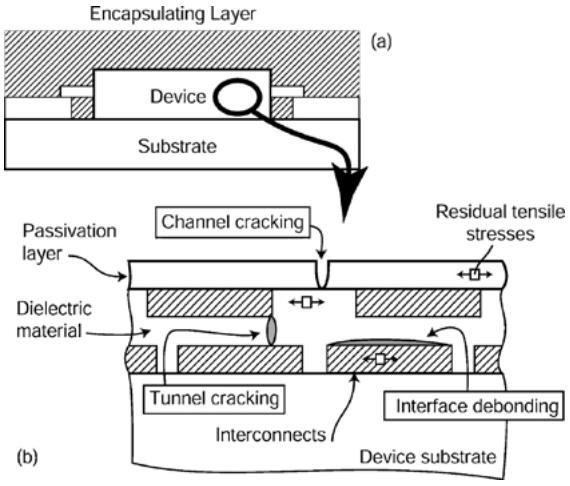

Figure 1. Schematic illustration of rectangular features: (a) at the device/packaging level, and (b) at the scale of features within a microelectronic device. Part (b) also illustrates cracking modes driven by tensile residual stresses.

When tensile stresses arise during deposition or due to differences in thermal expansion, likely failure modes include: (i) interface debonding along material junctions, (ii) channel cracking in layers bounded by a free surface, and (iii) tunneling cracks in materials bounded by adjoining layers (see Fig. 1b). In order to determine which mode of failure will be triggered, one must compare the driving forces for each crack to the appropriate fracture toughness (i.e. interface toughness or intrinsic (bulk) material toughness). The focus here is on interface delamination between different materials sections, since interfaces between disparate materials are typically much weaker than intact sections. Nevertheless, the prediction of tunneling cracks or channeling cracks *within* a material section is identical to interface debonding. One merely needs to consider the crack as occurring between two sections with identical elastic properties, and use the material's intrinsic toughness as the "interface" toughness.

We limit our attention to two-dimensional architectures with the assumption that the architecture does not vary in the out-of-plane dimension. This is appropriate in many applications, for example interconnects in microelectronics where line lengths greatly exceed cross-section dimensions. Two important cracking modes can be considered, as illustrated in Fig. 2: steady-state debonding in the out-of-plane direction (both along vertical and horizontal interfaces), and in-plane crack growth along an interface (where the direction of crack

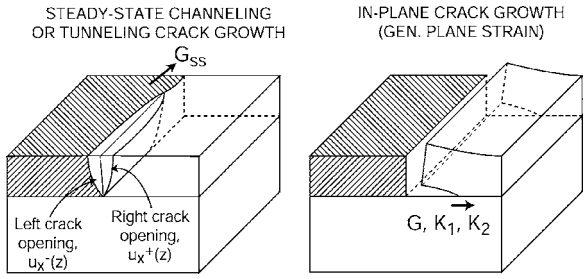

Figure 2. Illustration of the cracking modes analyzed using a two-dimensional analysis: steady-state cracking in the out-of-plane direction (left), and in-plane cracking along interfaces (right).

advance lies in the plane of the model). The mechanics framework needed to predict these types of failure is well established. The review article by Hutchinson and Suo [2] provides an excellent overview.

There have been several previous works that have treated cracking between material sections with finite in-plane dimensions in thin films: both finite-width strips [5] and periodic architectures [3]. A closely related study is the analysis of stresses in an elastic matrix surrounding a rigid square inclusion [6]. This work can be thought of as a specific example of the framework outlined here, with no consideration of crack driving forces but considerably more detail regarding stress distributions near the inclusion. Additionally, there have been numerous previous studies of debonding from material junctions, including those with finite crack lengths (e.g. [7]), three-dimensional interface corners (e.g. [8, 9]), and the edges of films or thin sections (e.g. [10–13]). These previous studies establish much of the theoretical framework needed to extend the energy release rate characterization described here to mode-dependent failure (i.e. approaches based on mixed-mode stress intensity factors).

In this paper, we consider out-of-plane debonding, as shown in Fig. 2(a). When considering out-of-plane cracks that channel or tunnel between adjacent sections, the crack driving force reaches a steady-state, wherein the energy released upon cracking is independent of the out-of-plane geometry. This occurs when the out-of-plane crack length exceeds about ten times the film thickness. (See [14] for a fairly comprehensive study of channeling cracks of finite length). The steady-state value, which is the maximum obtainable, can be computed by considering the energy released in converting thin slice of the intact section (ahead of the crack tip) into a cracked section (behind the crack tip). Naturally, the shape of the crack

tip and its mode-mixity is not captured using this approach.

Although not explicitly addressed in this work, the numerical approach set forth is equally appropriate for in-plane delamination, as shown in Fig. 2(b) (and covered by Yu and Hutchinson [15] for a single finite-width section bonded to a substrate). Specifically, the meshing strategy leads to the distribution of elements around the cracked interface needed to get accurate crack tip parameters (e.g. G, K_1, K_2).

However, as is well detailed elsewhere (e.g. [2]), two complications arise for arbitrary material combinations. First, the amplitude and spatial variation of the crack tip singularity depends on the elastic properties of the materials adjoining the singularity point. Secondly, the interface toughness is generally dependent on the mode-mixity, which also depends on the materials comprising the crack faces. Significant progress towards addressing the first of these can be made using interaction integrals to accurately characterize the near-tip behavior (e.g. [15]). The strategy described in the next section is ideal for these computations, as they include focused radial meshes at all crack tips. The second issue is far more challenging; interface properties are strongly influenced by fabrication techniques, which in turn are strong influenced by the desired geometry.

Although a fairly detailed theoretical understanding has been developed, a general framework for incorporating these behaviors into failure prediction has yet to be rigorously established. One of the key considerations for mixed-mode of interface failure is the size of K-dominated stress fields in relation to finite feature size and any intrinsic material length scale present in the material. Naturally, a fracture mechanics approach might not be valid if the asymptotic singular fields created by material junctions are limited to physical distances over which isotropic elasticity is not appropriate. In the present work, we consider only the energy release rate of the interface. This can be thought of as a global characterization of the likelihood of interface debonding, without explicit consideration of the length-scales needed to evaluate a fracture approach based on mixed-mode stress intensity factors.

2. Steady-State Out-of-Plane Interface Delamination

The steady-state energy release rate for a crack tunneling or along an interface can be found by computing the work associated with the complete relaxation of the tractions holding an intact interface. For elastic materials, the results depend only on the initial interface stress (when relative interface displacements are zero) and the displacements after cracking (when interface stresses are zero). The energy release rate can be found via the following expression:

$$G_{ss} = \frac{1}{2h}\int_0^h [\sigma(z)(u_n^+(z) - u_n^-(z)) + \tau(z)(u_t^+(z) - u_t^-(z))]\,dz \tag{1}$$

where z is the distance along the interface, σ and τ are the normal and shear stresses acting at the interface *before* cracking, and u_n and u_t are the normal and shear crack face displacements *after* cracking. h is length of the interface that is debonding and corresponds to the crack length. The superscript $(+/-)$ denotes each side of the interface since displacements are not necessarily symmetric.

Results for a blanket film with identical elastic properties to surrounding materials provide useful normalizations for results presented here. For a blanket film, the stress can be written as the sum of intrinsic stresses arising from deposition and those arising from thermal expansion mismatch with the substrate;

$$\sigma = -(1+v)\bar{E}\,\Delta\alpha\,\Delta T + \sigma^o \tag{2}$$

where the plane strain modulus of the film is $\bar{E} = E/(1-v^2)$; $\Delta\alpha = \alpha - \alpha_s$, where α and α_s are the thermal expansion coefficients (CTE) of the layer and substrate respectively, and ΔT is the change in temperature from the deposition temperature. σ^o is the intrinsic stress arising from sources other than CTE mismatch.

In cases considered here, σ^o is taken to be zero and a thermal strain (i.e. $\Delta\alpha\,\Delta T$) is specified for each section. It should be emphasized that the stress in a finite-sized section is not uniform (and hence not strictly given by Eq. (2))—only in the limit that the dimensions approach those of a blanket film. Further insight regarding the nature of stress distributions driving debonding in blanket film multi-layers can be found in [16]. The stresses arising in isolated thin strips with finite dimensions are discussed in [5, 17], while the stresses in embedded, periodic arrangements are discussed in [3]. Also, it should be noted that the singular stresses present at intact material junctions have been discussed in detail elsewhere (e.g. [8, 11, 13]). Regardless of the spatial distribution, the magnitude of the

stress in an intact section will be proportional to the result given as Eq. (2) (and the modulus of adjacent sections).

For purely elastic material response, the energy release rate for interface cracking will depend only on the residual stress in each section and not on its source (e.g. [1, 2]). Naturally, it does depend on the moduli of other material sections, particularly those adjoining the interface that is debonding (e.g. [1, 2]). A number of results for steady-state delamination pertaining to films can be written in the form:

$$G_{ss} = g\frac{\sigma^2 h}{\bar{E}} \tag{3}$$

where σ is the film stress driving delamination, h is the film thickness, and g is a dimensionless constant that depends on the crack configuration. Examples include: $g = 0.5$ for steady-state film delamination (i.e. crack growth parallel to the film along the interface, when the entire film peels off), $g = 1.976$ for a channeling crack in a blanket film perpendicular to the interface on a substrate with identical elastic properties, and $g = 0.785$ for a tunneling crack in a layer sandwiched between semi-infinite solids with identical elastic properties (e.g. [1, 2]). In this article, the latter two are relevant to steady-state delamination of finite-sized interfaces. They represent delamination along an interface of length h between two identical solids, when the stress normal to the interface is uniform and equal to σ.

3. Finite Element Implementation and Convergence Considerations

The principal goals of the finite element approach are to create a single meshing strategy that: (i) accurately captures stress and displacement fields near singularities arising at interfaces and corners, and (ii) can be used on arbitrary combinations of rectangular material sections. The approach outlined below provides an effective and reliable procedure to study interface behavior in complex geometries. Although more complex procedures can be developed to improve computational efficiency, the additional cost of implementation is usually not warranted given the current speed of computers. Unless great care is taken to separately address material junctions and crack tips, automatic mesh generation schemes very often lead to unreliable meshes near such singularities.

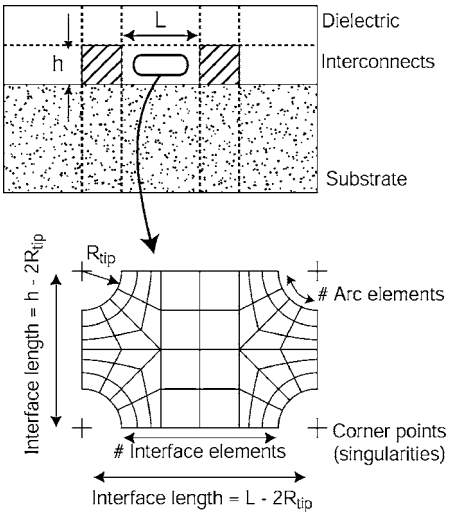

Figure 3. Overview of the meshing approach: each material block and sub-material block (defined by intersecting boundaries) contains focused radial meshes at the corners, with an artificial tip radius that is kept much smaller than other dimensions.

3.1. Strategy for Generating Finite Element Models

The general meshing strategy is illustrated in Fig. 3. Geometric lines along material interfaces are extended through the entire model, creating a collection of coherent rectangular "material blocks." Artificial material interfaces are created within a single material where true interfaces project through adjacent layers. These interfaces have no effect on the model, other than to aid in the generation of a coherent mesh. The nodes along these interfaces may either be removed, or retained to model cracking within a single material at these locations. This partitioning of the model into complete rectangular domains allows the application of a single meshing strategy developed for rectangular sections with arbitrary aspect ratios.

Each block of material (or sub-material block bounded by the same type of material) is meshed with focused radial fan meshes at the corners. The bottom of Fig. 3 illustrates the basic philosophy of the approach. The sides not connected to the corners are meshed with uniform elements that are easily connected to rectangular meshes, creating a coherent mesh within the material block. An artificial radius is introduced at each corner. This radius is kept small, such that the corner does not affect the results within a physically meaningful distance from the singularity. Alternatively, one could collapse the elements at the corners and create singularity elements. Generally speaking, there is not

much advantage to doing this, as the strength of the singularity at the corner depends on the adjoining materials, and different element types would be required for each corner combination. Moreover, by eliminating corner points in the numerical model, one avoids the formation and release of the multiple constraints tying materials together at the corner.

A comprehensive strategy to general finite element models can be based upon meshing the side of the smallest section first, since this will require the greatest mesh density of the model. All subsequent sides can then be referenced to this first section. Obviously, this is a brute force approach that results in far greater mesh densities than are absolutely needed in larger sections. Moreover, this approach is obviously not computationally efficient from the standpoint that focused meshes are not strictly required at every material junction—only those where cracking is likely to occur. However, it is often difficult to identify these locations a priori, and the approach described here allows for any number of interfaces to be debonded simultaneously, or sequentially.

The key feature is that convergence studies are not needed for each type of failure, since the limiting feature size governs the model generation. Despite any meshing inefficiency, model generation and solution is rapid for sections involving ten to thirty or so sections. For the examples presented here, mesh generation is achieved on the order of seconds, and solutions are generated on a standard personal computer (e.g. 2 GHz chip speed, 1 GB RAM) in several minutes.

3.2. *Convergence Considerations and Meshing Parameter Guidelines*

To illustrate guidelines for mesh characteristics that allow generally accurate results, we present a study of delamination along an interface contained in a single layer (as shown in Fig. 2(a)). This simple case has both a triple-junction singularity at the bottom of the layer, and a free surface singularity at the top of the layer. Since the required mesh density increases slightly with modulus mismatch, results are shown for a relatively large difference in the moduli within the layers. Results are presented for $E_1 = E_s = 20E_2$, where E_s is the elastic modulus of the substrate, and E_1 and E_2 are the elastic moduli of the top sections. (The Poisson's ratio of all sections is taken to be 1/3.) The results in this section were generated using conventional eight-noded isoparameteric quadrilateral plane strain elements; similar results can be generated for any element type.[1]

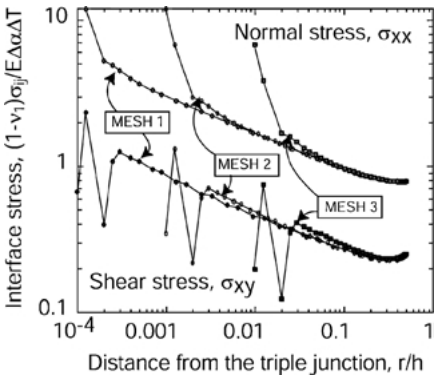

Figure 4. Interface stress distributions near a triple junction from several meshes. Note that the stresses are less singular than $r^{-0.5}$ and convergent, accurate stresses are obtained for locations larger than about ten times the artificial tip radius.

Figure 4 illustrates that the corner radius has a completely controllable effect on the resulting computations. The interface stress prior to cracking along the bimaterial interface is shown for three different meshes, each with a different tip radius ($r/h = 10^{-4}$, 10^{-3} and 10^{-2}) and the same number of elements along the interface. It is clear that the stress along the interface can be obtained to within an arbitrarily small distance from material triple junctions by decreasing the radius of the artificial notch. Note that the results have been truncated near the free surface ($r \sim h$) for clarity purposes; in general there is a weak singularity there when there is a modulus mismatch between the sections (see for example [11]).

Using a single mesh generation algorithm, one can rapidly develop guidelines for appropriate meshing parameters, based on the size of the smallest material section (or sub-block). The goal is to identify the following parameters: (i) the required size of the tip radii such that they do not effect the results, (ii) the number of elements in the fan region surrounding each corner, and (iii) the number of elements required along each interface.

Figure 5 depicts the percentage error in the energy release rate as a function of meshing parameters, defined as the difference between the result with various meshes and the value obtained from the finest mesh. (We present results for ubiquitous eight-noded quadrilaterals; four-noded quadrilateral yield similar results, with slightly smaller required element sizes.) Results are shown for two types of calculations: the dashed

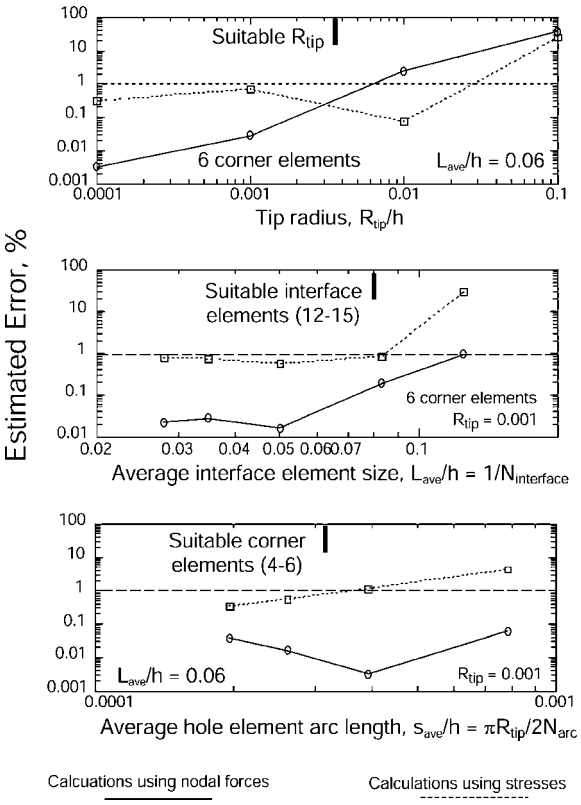

Figure 5. Convergence studies on energy release rate for a channeling interface crack as shown in Fig. 4: the radius of the artificial notch at material corners (top), the average element size along the interface (middle) and the element size/number in the fan mesh focused at the corner (bottom).

lines correspond to using nodal constraint forces and nodal displacements, while the solid lines correspond integrating the product of the interface stresses (taken as the average value at the centroid) and the nodal displacements.

As one would expect, using nodal forces is more efficient, since these values correspond directly to those minimized in the finite element method. By contrast, element averaged stresses introduce slightly more error due to the averaging over the element volume. While nodal forces are obviously preferred, averaged stresses may facilitate post-priori evaluations of Eq. (1) when using commercial or in-house finite element analysis codes.

The regions below the dashed line in Fig. 5 correspond to less than 1% difference with the results for a finely detailed mesh containing more than 10,000 elements. Convergence studies on a channeling crack in a uniform film demonstrate that similar benchmarks are obtained using analytical solutions (i.e. $g = 1.976$ in Eq. (3)). Results such as these can be used to develop guidelines for tuning the mesh generation algorithm to yield acceptable results with a minimum of cost.

The thresholds for mesh parameters used in a previous study (Ambrico, Jones and Begley, 2002) are illustrated in Fig. 5. Generally speaking, the results are independent of the artificial tip radius for radii two orders of magnitude smaller than the interface length. Using 12–15 elements along the interface and 4–6 elements in the fan surrounding the corner produces results that are insensitive to details of the mesh. It is interesting to note the calculations are often very insensitive to the number of elements around the corner, particularly if nodal constraint forces are used.

4. Interface Debonding Around Rectangular Inclusions

To illustrate the usefulness of the approach described above, we present results for debonding along the sides of a rectangular inclusion. The model is shown in Fig. 6. A rectangular block of variable dimension is subjected to a thermal strain; the surrounding matrix is free of thermal strain. Periodic boundary conditions are applied on either vertical edge, such that the model represents a unit cell out of a row of embedded inclusions (such as might occur for interconnects in microelectronics). The bottom of the cell is fixed to have zero vertical displacements, while the top remains free to contract. The calculations were performed using a

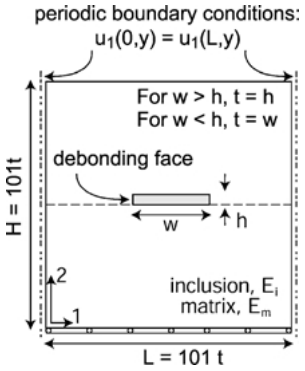

Figure 6. Model for studying debonding around square inclusions; the outer dimensions are fixed relative to the smallest dimension of the inclusion; the inclusion has a uniform thermal strain imposed, while the surrounding material is initially stress-free.

commercial code that incorporates the model generation technique outlined above [18]. The code uses four node quadrilaterals and mesh parameters slightly smaller than those shown in Fig. 5 (with convergence determined in a similar manner). Generally speaking, the models in this section had three to five thousand elements.

It should be noted that these boundary conditions create large interface tractions along the vertical interfaces, while those along the horizontal interfaces are negligible except near the corner singularities. At the corners, the opening displacements are small (for a single edge debond); as such, the energy release rate for the top and bottom face debonding is several orders of magnitude smaller than the sides. Alternatively, one could constrain both top and bottom outer edges of the entire system to create large interface stresses on all sides. However, the examples presented here are motivated by sections attached to a substrate and subsequently covered. In such cases, the substrate provides constraint only in the lateral direction.

The energy release rate for debonding of one vertical face is shown in Fig. 7 as a function of inclusion dimensions. The energy release rate is normalized by $\sigma^2 h/\bar{E}$, where σ is given by Eq. (1) (with $\sigma^o = 0$). $\bar{E}_i$ is the plain strain modulus of the inclusion. Results are shown for several values of modulus for the surrounding matrix: $\bar{E}_m/\bar{E}_i = 1, 2.8, 8$. It should be emphasized that the period length, which corresponds to inclusion spacing, is kept fixed relative to the smaller of the inclusion dimensions. So, for $w/h < 1$, where w/L is held fixed and h/L increases, the spacing between debonding interfaces is decreasing (relative to the period). Thus, the energy release rate drops as the crack density increases.

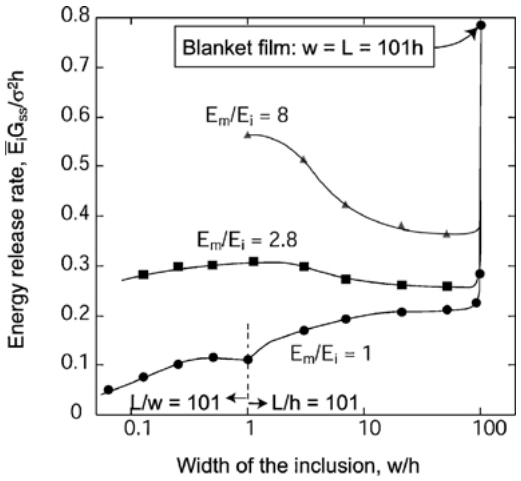

Figure 7. Energy release rate for debonding along one side of a rectangular inclusion (shown in Fig. 6) as a function of inclusion dimensions.

For $w/h > 1$, where h/L is held fixed and w/L increases, the distance between a debonding interface and the intact edge of the adjacent inclusion is decreasing. The key result is that debonding releases strain energy in both inclusions. In the limit that w approaches L (i.e. $w/h = 101$), the inclusion becomes an intact film, and one recovers the result for a tunneling crack in a sandwich layer. This is necessarily much higher, since one crack relieves strain energy on both sides of the interface, as opposed to just one for moderate w/h. The interplay between debond and feature spacing is discussed in more detail in [3] for interfaces between sections contained in a single layer. In this work, specific attention is placed on explaining the sharp increase in energy release rate as two adjacent sections are placed very close together (e.g. Fig. 7 for $w/h \to 101$).

For *blanket films*, increasing the modulus of the surrounding material decreases the energy release rate. This is because stiffer adjacent sections provide more constraint near the crack tip and reduce crack opening displacements. Note that one layer's modulus does not affect the stress in adjacent layers, which is dictated solely by expansion mismatch with the substrate. However, for *finite-sized sections*, the material on the sides of the inclusion *does* affect the stress in the intact section and specifically, the interface that debonds. For widely spaced features relative to the section height, the net effect is higher energy release rates for debonding. Conversely, the energy release rate is lower than the blanket film result for narrowly spaced features relative to the section height. Lower energy release rates due to constraints imposed by stiff adjacent sections occur only for inclusions whose width is nearly equal to the inclusion period. Finally, it should be emphasized that one obtains different limits (i.e. different trends with aspect ratio) for single isolated inclusions (in contrast to the periodic spacing considered here).

5. Concluding Remarks

The procedure outlined above is useful not only in identifying interfaces that are prone to debonding, but also in identifying failure sequences that are triggered by

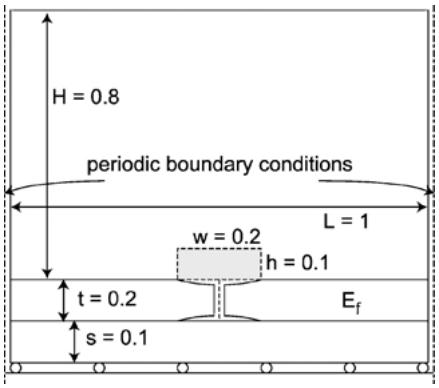

Figure 8. Schematic of a three-layer system used to illustrate the effects of constraint loss induced by debonding near finite sized features.

debonding. As an example, consider the simple geometry shown in Fig. 8, which depicts a finite section bonded on top of a blanket film. Both of these sections are then encapsulated by top and bottom layers, with elastic moduli equal to five times the blanket layer. Only the layer with thickness t is under residual stress. The crack in the middle can be thought of as a tunneling crack in either a uniform film or along an interface separating two materials with roughly the same elastic properties.

As pointed out in earlier work [2], any source that reduces the constraint experienced by a cracking interface serves to increase the driving force. For the geometry shown in Fig. 8 *but without the inclusion*, the energy release rate for a channeling crack in the center of the middle layer is $\bar{E}_f G_{ss}/\sigma^2 t \sim 0.7$. If the inclusion has a modulus roughly five times lower than the film, it provides less constraint to hold the crack shut, and $\bar{E}_f G_{ss}/\sigma^2 t \sim 0.9$. If the underside of the inclusion is subject to debonding, the energy release rate for the crack in the adjacent layer jumps again to $\bar{E}_f G_{ss}/\sigma^2 t \sim 1.1$, due to the greater crack openings allowed by the debonded interface. Finally, if the bottom interface debonds in the same manner as the top face (as drawn in Fig. 8), the energy release rate is $\bar{E}_f G_{ss}/\sigma^2 t \sim 1.3$. In this last example, the increase in channeling crack driving force scales with the width of the feature, since the length over which strain energy is released in the middle layer increases. This indicates that debonding along relatively wide features will promote cracking in adjacent layers; the energy release rate can easily be more than double the value for cracking in a blanket film.

Although these results are obviously quantitatively applicable to the specific dimensions and properties given above, the example serves as excellent illustration of how finite-sized features can trigger unanticipated cracking mechanisms. (A further example is considered in [3], in which compliant and/or stressed sections dramatically increase the driving force for cracks in adjacent layers.) The numerical technique described in here is particularly attractive for failure sequences that involve debonding along multiple interfaces (such as those shown in Fig. 8).

Since each interface and material junction (or corner) is meshed appropriately, there is no need to regenerate model information between each analysis. Moreover, it is simple to incorporate a wide variety of boundary conditions. For example, constraints against vertical contraction would create larger driving forces along the top and bottom of the features. Moreover, the techniques presented here can be applied to any generic two-dimensional planar problems. By changing the element type and constraining the edges, one would easily model debonding in a thin layer with features distributed in the plane of the model (i.e. a top view of Fig. 2).

Note

1. Eight-noded quadrilaterals are the default choice in most finite element analyses; however, four noded quadrilaterals often perform better near singularities, particularly for non-linear material response.

References

1. J.L. Beuth, International Journal of Solids and Structures **29**, 1657 (1992).
2. J.W. Hutchinson and Z. Suo, in *Advances in Applied Mechanics*, edited by J.W. Hutchinson and T.Y Wu (Academic Press, San Diego, 1992), Vol. 29, p. 63.
3. J.M. Ambrico, E.E. Jones, and M.R. Begley, International Journal of Solids and Structures **39**, 1443 (2002).
4. X.H. Li, Z. Suo, Q. Ma, and H. Fujimoto, Engineering Fracture Mechanics **66**, 387 (2000).
5. H.-H. Yu and J.W. Hutchinson, Thin Solid Films, 54 (2003).
6. E.D. Reedy and T.R. Guess, International Journal of Solids and Structures **38**, 1281 (2001).
7. A.R. Akisanya and N.A. Fleck, International Journal of Solids and Structures **34**, 1645 (1997).
8. P.E.W. Labossiere and M.L. Dunn, Journal of the Mechanics and Physics of Solids **49**, 609 (2001).
9. P.E.W. Labossiere, M.L. Dunn, and S.J. Cunningham, Journal of the Mechanics and Physics of Solids **50**, 405 (2002).
10. X. Liu, Z. Suo, and Q. Ma, Acta. Materilia. **47**, 67 (1998).

11. N.W. Klingbeil and J.L. Beuth, Engineering Fracture Mechanics **66**, 93 (2000).
12. E.D. Reedy and T.R. Guess, International Journal of Solids and Structures **39**, 325 (2002).
13. A.R. Akisanya and C.S. Meng, Journal of the Mechanics and Physics of Solids **51**, 27 (2003).
14. J.M. Ambrico and M.R. Begley, Thin Solid Films **419**, 144 (2002).
15. T. Nakamura and D.M. Parks, International Journal of Solids and Structures **25**, 1411 (1989).
16. M. Finot and S. Suresh, Journal of the Mechanics and Physics of Solids **44**, 683 (1996).
17. A. Wikstrom, P. Gudmundson, and S. Suresh, Journal of the Mechanics and Physics of Solids **47**, 1113 (1999).
18. TCA Solutions, LLC, *LayerSlayer Software*, www.tcasolutions.com, 2003.